The relationship between fracture toughness and tensile properties of A357 cast aluminum alloy

N.D. Alexopoulos[1*] and *M. Tiryakioğlu*[2]

October 28, 2008

[1] University of the Aegean

Department of Financial and Management Engineering

821 00, Chios

Greece

E-mail address: nalexop@tee.gr

[2] Robert Morris University

Department of Engineering

Moon Township, PA 15108

USA

E-mail address: tiryakioglu@rmu.edu

[*]Corresponding author

Abstract

The fracture related mechanical properties of the A357 cast aluminum alloy, namely elongation to fracture, tensile strain energy density (tensile toughness), strain-hardening exponent and plane strain fracture toughness were investigated. Correlations between these properties have been established for 25 different artificial aging heat treatment conditions and for 5 minor variations in chemical composition. Empirical relationships between strain energy density and tensile elongation to fracture and strain-hardening exponent have been developed. Analysis of the fracture surfaces indicated that the fracture mechanism of the investigated specimens varies according to the artificial aging conditions. Moreover, empirical relationships between fracture toughness and strain energy density as well as between fracture toughness and strain-hardening exponent have been developed, which can be used to estimate the plane strain fracture toughness of A357 as a function of yield strength and tensile toughness.

Keywords: Cast aluminum alloys; tensile test; fracture toughness; strain hardening exponent; intrinsic toughness.

1 Introduction

Despite the progress made in the last two decades in improving the molten metal quality and process design concepts, low levels of ductility and fracture toughness, usually accompanied by high scatter in these properties, compared to the respective wrought aluminum alloys, still represent significant drawbacks for increased use of aluminum castings in aerospace applications. Tighter controls currently applied during the casting process have resulted in reduction in structural defects in castings, i.e. pores and oxide bifilms, which seriously degrade mechanical properties [1, 2]. With increasing structural quality of castings, aluminum castings are expected to be used more commonly in critical applications.

The demands for improved damage tolerance of cast aluminum alloys have increased the importance of fracture related properties. In critical aerospace applications, certain mechanical properties of cast aluminum alloys, such as the yield strength R_p, the elongation to fracture A_f and the plane strain fracture toughness K_{cr}, should exceed minimum values to be considered for selection. In non-critical applications, fracture toughness tends to be neglected, and tensile properties are emphasized.

A review of the literature has shown that there are limited data on fracture toughness of cast Al-Si alloys. There are several reasons for this limited number: (i) the fracture toughness test, due to its complexity, is usually not performed, instead 'faster' mechanical tests, e.g. the hardness and tensile tests are preferred to evaluate the mechanical performance of these alloys, (ii) in several studies, e.g. [3,4] valid K_{Ic} values could not be obtained mainly because of the thickness requirement, and (iii) like all fracture-related mechanical properties, fracture

toughness is strongly affected by the presence of structural defects, e.g. pores and oxides that may lead to unrealistically low results. Consequently, K_{Ic} values obtained in different studies indicate a large scatter in fracture toughness.

The most widely used cast aluminum alloy in the aerospace industry is the age-hardenable A357 (Al-7% Si-0.6% Mg). The A357 cast alloy with minor modifications in chemical composition has been extensively investigated in recent research projects, e.g. [5–7] and in several articles of the open literature, e.g. [8–15]. Nevertheless, there is still a need to investigate the tensile properties and fracture toughness of A357, as well as correlations between the results of two tests. This study is motivated by this need. Results from continuously - cast specimens, that do not contain the structural defects commonly observed in shape castings, are reported.

2 Background

Several equations have been proposed in the literature to estimate the fracture toughness of several aluminum alloys from other mechanical tests, such as the impact or the tension test, e.g. [16–19]. In the pioneering work, Hahn and Rosenfield [16] introduced an equation relating K_{Ic} to tensile properties:

$$K_{Ic} = \sqrt{\frac{2 \cdot \delta \cdot E \cdot R_p \cdot \varepsilon_f}{(1-\nu^2) \cdot \beta}}, \tag{1}$$

where δ is the plastic zone width, ε_f is the true tensile fracture strain, β is a constant which is equal to 3 for plane strain conditions, E is the modulus of elasticity, R_p is the

yield strength and ν is the Poisson's ratio of the alloy. As the strain hardening mechanism tends to distribute the developed strain on a micro level, the parameter δ becomes larger with increasing the strain-hardening exponent n, provided that the material follows the well-known Ludwik-Hollomon equation:

$$\sigma = H \cdot \varepsilon^n. \tag{2}$$

In the above equation, σ is the true stress, H is strength coefficient, ε is the true strain and n the strain-hardening exponent. Hahn and Rosenfield, using their experimental data obtained on steels, titanium alloys and aluminum alloys, observed that $\delta = k \cdot n^2$, with k = 0.0254 m (1 inch) in their original work. Inserting the above equation of δ into equation (1), the plane strain fracture toughness is related to strain-hardening exponent n, as:

$$K_{Ic} = n \cdot \sqrt{\frac{2 \cdot k \cdot E \cdot R_p \cdot \varepsilon_f}{(1-\nu^2) \cdot \beta}}. \tag{3}$$

In equation (1), the K_{Ic} value is related to the $\sqrt{R_p}$, thus implying that fracture toughness would increase with yield strength. However, it has been shown, e.g. [18,20,21], that fracture toughness decreases linearly with increasing yield strength for various aluminum alloys. This linear, negative correlation is due to the fracture strain both decreasing with increasing yield strength, as recently discussed by Kamp et al. [22].

There have been several attempts to apply equation (3) to cast Al-Si aluminum alloys. Tagami et al. investigated Al-10Si-3Cu-0.3Mg [23] and Al-7Si-0.5Mg cast alloys [24] and correlated the fracture toughness of these alloys with their tensile behavior. The authors

modified equation (3) as:

$$K_{Ic} = B \cdot n \cdot \sqrt{R_p}, \tag{4}$$

where B is an empirical constant that takes the value of 13.1 $(\text{MPa}\cdot\text{m})^{1/2}$ in the original work of Tagami et al. Terjesen [25] investigated the relationship between tensile and fracture toughness test results for an Al-10Si-0.36Mg cast alloy in the T6 condition. Terjesen found that equation (4) provided the best fit to the experimental data in [25], when the empirical constant takes the value of $B = 17.66$ $(\text{MPa}\cdot\text{m})^{1/2}$.

Peel and Forsyth [26] assumed that the elastic strain energy release rate per unit crack length and per unit thickness is balanced by the plastic work done:

$$W_p = 2 \cdot r \cdot W, \tag{5}$$

where r is the radius of the plastic zone at the advancing crack tip and W is the strain energy density (or tensile toughness). W is a tensile property that can be evaluated from the area under the tensile stress - strain flow curve as:

$$W = \frac{dU}{dV} = \int_0^A \sigma \cdot d\varepsilon, \tag{6}$$

where U is the strain energy, V the material volume and A the elongation just before fracture and hereafter will be called elongation at fracture. Assuming that the metal follows the Ludwik-Hollomon equation, this plastic work can be expressed with the aid of eqns.(2)

and (6), as:

$$W_p = 2 \cdot r \cdot \int_0^{\varepsilon_f} H \cdot \varepsilon^n \cdot d\varepsilon = \frac{2 \cdot r \cdot H \cdot \varepsilon_f^{n+1}}{n+1}, \tag{7}$$

where ε_f is the true fracture strain. Peel and Forsyth considered that for the critical condition at the onset of fracture in the toughness test the elastic energy W_e released as the crack grows equals the amount of plastic work W_p needed to strain the crack-tip zone to the point of fracture. The released energy W_e can be related to the fracture toughness as

$$W_e = \frac{K_{Ic}^2(1-\nu^2)}{E}, \tag{8}$$

Since $W_e = W_p$, eqns(7) and (8) give the fracture toughness dependence with the strain-hardening exponent n:

$$K_{Ic}^2 = \frac{E}{(1-\nu^2)} \cdot \frac{2 \cdot r \cdot H \cdot \varepsilon_f^{n+1}}{n+1}, \tag{9}$$

where ν and E are the material's Poisson ratio and modulus of elasticity, respectively.

Yeong et al. [27] stated that strain energy density W characterizes the damage tolerance potential of a material and may be used to evaluate the material's fracture under both, static and fatigue loading conditions. Sih et al. [28, 29] noted that energy density may be directly related to K_{Ic}, which evaluates the fracture of a cracked member under plane strain loading conditions. The quantity $\frac{dU}{dV}$ in equation (6) tends to a critical value of energy density W_c as the elongation tends to the value of elongation at fracture A just before the failure time. According Sih et al. [28,29], the critical energy density function may be related to the energy

density factor S:

$$\left(\frac{dU}{dV}\right) = \frac{S}{r} \rightarrow \frac{S_c}{r_c}, \tag{10}$$

and at the time of instability, just before fracture occurs:

$$W_c = \frac{S_c}{r_c}. \tag{11}$$

Note that the plane strain fracture toughness value K_{Ic} gives S_c, since:

$$S_c = \frac{(1+\nu)\cdot(1-2\cdot\nu)\cdot K_{Ic}^2}{2\cdot\pi\cdot E}. \tag{12}$$

The critical ligament size r_c of equation (11) measured from the crack tip is related to the process zone size that has been discussed extensively in the literature. Crack initiation is assumed to prevail when $\frac{dU}{dV} \rightarrow (\frac{dU}{dV})_c$ while the onset of rapid crack propagation is assumed to be reached when $S \rightarrow S_c$ [27, 28]. Substituting the critical energy factor S_c of equation (11) to equation (12), the plane strain fracture toughness K_{Ic} becomes a function of the strain energy density W, as:

$$K_{Ic}^2 = \frac{2\cdot\pi\cdot E\cdot r_c\cdot W}{(1+\nu)\cdot(1-2\cdot\nu)}. \tag{13}$$

Barson and Rolfe [17], proposed an empirical equation to estimate K_{Ic} from known Charpy V-notch impact energy W_{CVN} and tensile yield strength R_p values:

$$\left(\frac{K_{Ic}}{R_p}\right)^2 = a\cdot\left(\frac{W_{CVN}}{R_p}\right)^2 + b. \tag{14}$$

The a and b coefficients are both, empirical and material dependent constants. This empirical equation was originally applied successfully to low-alloyed and austenitic steels. Later, Equation (14) has been used extensively for the fast estimation of the alloy's fracture toughness from easy to perform mechanical tests, such as the tensile and the impact test.

3 Experimental investigation

The material used for the fracture related mechanical properties investigations was A357 cast ingot aluminum alloy and A357 cast aluminum alloy with minor variations in chemical composition. The A357 ingots were supplied by Pechiney, France and were cast with continuous casting process as rods. The use of ingots has been preferred to keep structural defects such as porosity and other inclusions minimal and, hence, to minimize scatter in mechanical properties. The chemical composition of the delivered ingot was Al-7.0Si-0.55Mg-0.10Ti-0.12Fe-<0.10Mn. For the experimental investigation, specimens for microstructural characterization and tensile tests were cut from the middle section of the ingots to obtain the same solidification conditions. The cast alloys with variations in chemical composition were produced by Ciral, France by exploiting the patented casting method SOPHIA in the framework of the European BRITE/EURAM research project ADVACAST [5]. The test program included the addition of 1% Cu to the 'reference' A357 aluminum alloy. Further modifications were made by adding to the Cu-modified alloy, different minor alloying additions, namely Ag, Sm or Sr. Specimens for microstructural characterization, tensile and fracture toughness tests were cut from the middle section of a 30 mm thickness cast plate.

The tensile specimens were machined according to the ASTM E8M specification with 5 mm thickness and 12.5 x 50 mm being the reduced cross section of the specimen. The fracture toughness specimen configuration was a C(T) specimen according to the ASTM E399 standard of 40 x 48 mm and 20 mm thickness. Both specimen configurations can be seen in Figure 1.

The cast ingot specimens were solution heat treated for 22 hours at 540°C and quenched in cold water <10°C. Artificial aging of the specimens was conducted at the temperatures 155, 175 and 205°C which cover the range of temperatures involved for artificial aging of commercial A357 cast alloys, e.g. [21, 30]. In the Cu-modified alloys, two different quenchants were used; (i) cold water quench with ice <10°C (hereafter called I/T) and (ii) 20% aqueaous polyalkylene-glycol solution (hereafter called G/T). The copper modified A357 alloys followed solid solution heat treatment procedures based on extensive thermodynamic calculations and experiments, as outlined in Table 1. The artificial aging heat treatment conditions were 20 hours at 155°C for the A357 cast alloy, while for all the copper modified alloys were 8 hours at 170°C.

The tensile tests were carried out according to ASTM E8M with a constant deformation rate of 3.3×10^{-4} s^{-1}. A data logger was used to store the data in a digital file. To get reliable average values of the tensile mechanical properties, a minimum number of six tensile tests have been carried out. In total, 154 tensile tests were performed and evaluated for the various artificial aging conditions of the A357 alloy [31, 32], while 135 tensile tests were evaluated for the different chemical modifications of the A357 alloy [5]. The evaluated properties were: yield strength R_p (0.2% proof stress), tensile strength R_m, elongation to fracture A_f (ASTM E8M) and strain energy density W (tensile toughness). True stress-true strain curves of the specimens were computed based on the conservation of volume in the uniform elongation regime. Strain energy density was calculated for each specimen using Reimann sums.

The fracture toughness tests were performed according to ASTM E399 in the University

of Lisboa, in the framework of the research project ADVACAST [5]. Three tests had been performed per chemical modification in order to get an average value and in total 24 tests had been carried out. The force - crack opening displacement curves were recorded in a digital file. The fracture toughness values were evaluated by exploiting the compliance method according to the standard ASTM E399. More details can be found in the respective report of the project [5].

To characterize the predominant fracture mechanisms of the investigated A357 cast ingot tensile test specimens, fracture surfaces were analyzed, using a Phillips FEG/SEM XL40 scanning electron microscope, with an operating voltage of 20 kV equipped with an EDX system.

4 Experimental results

4.1 Different artificial aging conditions

Typical microstructures of the investigated A357 cast ingot aluminum alloy for the W-temper and various artificial aging heat treatments are presented in Figure 2. The microstructure consists of the Al matrix and the Si particles. Note that the Si particles are round and somewhat hexagonal. The size of the Si particles was quantified by digital image analysis using the ImagePro software. The average particle area was found to be approximate 8 μm [33]. Statistical analysis showed that the particle area and aspect ratio follow the lognormal distribution [33]. The secondary dendrite arm spacing of the alloy was measured to be approximately 27 μm.

Typical true stress - true strain curves for various artificial aging conditions of the cast aluminum alloy A357 can be seen in Figure 3. The strain-hardening exponent n values were calculated for all investigated heat treatment conditions and the results are presented in Figure 4. As expected, the strain-hardening exponent n value is decreasing from the initial value of 0.21 to 0.05 with the increase of the artificial aging time (under-aged condition). The n values are reaching a plateau of the approximate values of $n = 0.05$ to 0.04, where the alloy is at its peak-strength condition. By further aging the alloy (over-aging condition), the n values are increasing, e.g. aging at 205°C in Figure 4.

Figure 5 shows the experimental results of the strain-hardening exponent n and elongation at fracture A values versus yield strength. For both properties in the under-aging condition, the decrease is linear with the increase in the yield strength. It is also evident

that this decrease follows almost the same rate (approximate the same linear decrease). For the condition of peak strength, minimum values of n and A are observed, as expected. By further aging the alloy (over-aging condition), both properties are increased.

Analysis were performed [32] to investigate whether the fracture mechanism changes with the various artificial aging conditions. Fracture surfaces from various tensile specimens are presented in Figure 6. The specimens involved in the analysis were from W-temper, Figure 6(a), under-aging in Figure 6(b) (16 hours at 155°C) and peak-aging conditions in Figures 6(c) and (d) (48 hours at 155°C and 16 hours at 205°C), respectively. For all the artificial aging conditions investigated, rough fracture surfaces including large dimples were observed indicating that extensive plastic deformation has taken place prior to final fracture.

The SEM images presented in Figure 6, shows the same ductile fracture for all investigated cases. Figure 7(a) shows in higher magnification a typical ductile fracture surface consisting of dimples. The point indicated by the arrow with the small rounded particles was found to contain high percentage of Al and some Mg and Si, Figure 7(b). Due to the low Si amount, the region was interpreted as the matrix metal strengthened by the β'' phase, which is a precursor to Mg_2Si.

Figure 7(c) shows a SEM image of an underaged specimen (aged for 48 h at 155°C). In addition to the fine dimples and cavities, micro cracks (as indicated by arrow) and flat, smooth surfaces were also observed on fracture surfaces. Using the EDX analysis, it was found that the indicated cracked area contained high amount of Si, as shown in Figure 7(d).

4.2 Modifications in chemical composition

The alloys had been cast with two processes, the normal investment casting process and the patented SOPHIA process [5] that enables high solidification rates, up to 700 K/min, depending on the thickness of the structure. In addition, different thickness had been casted, e.g. 5 mm, 10 mm, 20 mm and 30 mm, to measure the resulting Dendrite Arm Spacing (DAS) of the alloy. Typical micrograph of the microstructure of the A357 alloy casted with the patented process for the 5 mm plate can be seen in Figure 9(a). The DAS measured was 45.3 μm, while for the normal process was 68.5 μm. For the case of the 30 mm plate, out of which the fracture toughness specimens were machined, the DAS measured for the normal plate was 81.5 μm, while for the SOPHIA process only 50.0 μm. The results of the measured DAS can be found in Table 2.

Typical microstructure of the cast A357 alloy can be seen in Figure 9(a). The microstructure consists of the Al matrix and the Si particles, with the Si particles being somewhat fibrous. The size of the Si particles were quantified by digital image analysis using ImagePro software and average area was found to be approximate 9 μm. The addition of 1% Cu on the A357 alloy aimed to enhance strength due to the excellent aging behavior of the alloying element copper. For the high solidification rates that the SOPHIA process enables, the morphology of the Si particles almost have the same morphology than in the case of the base - A357 alloy, Figure 9(b). In the case of the normal casting process, a more lamellar structure of the Si particles was achieved that resulted in high notch effect. Consequently, mechanical properties were lower. The mean size of the Si particles was measured to be 9.5 μm.

Other minor alloying additions to the Cu-modified A357 alloy aimed to change the eutectic microstructure of the alloy, to enhance the ductility and fracture toughness properties. The small addition of silver (Ag) influenced the eutectic microstructure, only at the very low solidification rates (normal casting process). The lamellar, plate-like Si particles, which can be seen at the alloy A357+1% Cu for this solidification rate, coarsen due to the silver addition. However, for the higher solidification rates of the current SOPHIA process, no major difference in the eutectic structure was detected, Figure 9(c). The mean size of the Si particles was measured to be 13.2 μm.

The additions of Sm or Ag + Sm, had an influence on the eutectic Si-structure only in specimens that solidified at low rates. In those specimens, the formation of plate-like silicon structures for Cu-modified alloy was suppressed by the Sm addition. At high solidification rates however, the suppression of the lamellar Si structure in the alloy A357+1% Cu + Sm could not be observed, Figure 9(d). Furthermore the addition of Sm resulted in coarsening of the Si particles, having mean size 14.4 μm.

The mechanical properties of the cast aluminum alloys with variations in chemical composition can be seen in Figure 10. The yield strength $R_{p0,2\%}$, the tensile strength R_m, elongation to fracture A_f are presented in Figure 10(a), as well as both, strain energy density W and fracture toughness K_{Ic} values in Figure 10(b). Briefly, the 'reference' alloy A357 represents a well-balanced alloy of medium strength properties and high ductility - fracture toughness values.

The addition of 1% copper to the Al-7% Si system leads to enhanced response to artificial aging, due to the formation of an additional strengthening phase, θ'' (Al_2Cu) and possible

s′ (Al_2CuMg). This improvement in strength was accompanied by some reduction in both, ductility and fracture toughness values, Figure 10. For example, the copper addition in G/T quench increased the properties R_p and R_m by 9 and 11 MPa, respectively. Nevertheless, the elongation to fracture A_f and fracture toughness K_{Ic} values decreased by 56% and 15%, respectively.

The addition of the alloying elements Ag and Sm to the copper modified A357 alloy did not result in higher mechanical properties. Figure 10(a) shows that yield and tensile strength are at best marginally higher than those achieved with the Cu-modified alloy.

Strontium was expected to improve slightly the ductility of the material, due to the formation of 'globular' eutectic structure [34]. The resulting microstructure was very encouraging and the fibrous morphology of the Si particles was cancelled. This had an immediate impact on the ductility, which was shown by the tensile tests. As can be seen in Figure 10, the small addition of Sr to the copper modified alloy, increased by almost 50% the elongation to fracture A_f. However, the resulting microstructure did not increase fracture toughness.

The strain hardening exponent n for all cast alloys have been calculated from the respective tensile curves. The results are presented in the Figure 11. The Cu addition to the reference alloy almost halved the n value. Nevertheless, the n value is a function of the material's heat treatment condition, and a direct comparison may lead to unrealistic results.

5 Discussion and analysis of the results

5.1 Different artificial aging conditions

Gurland et al. [35,36] indicated that the two-phase aluminum-silicon alloys fail by ductile fracture in three stages: (i) crack initiation within silicon particles, (ii) growth of these cracks into cavities, and (iii) rupture of aluminium rich matrix separating the cavities. Doglione et al. [37] made in-situ observations on the damage accumulation to Si particles during a tensile test. They observed that for the high-quality cast alloys with small SDAS, the numerous and highly-branched interdendritic channels disperse microcracks and consequently delay the final fracture. On the contrary, Meyers et al. [38] stated that they did not observe fracture at Si particles followed by microvoid growth and coalescence as the primary failure mechanism. This mechanism was also observed in the investigations performed in the works in [39, 40]. Tan et al. [41] performed fracture toughness tests on A357 specimens. Mainly, they observed the same mechanism of void growth and coalescence of the submicron-strengthening particles that resulted in the growth of the main fracture crack. However, they also noticed that when the silicon particles become more spherical and smaller, the intergrannular fracture mode and the fractured silicon particles were replaced by the conventional ductile rupture.

For the underaged specimen of 48 h at 155°C, in addition to the fine conventional ductile rupture (dimples and cavities), also micro cracks and flat, smooth surfaces were observed. The flat and smooth surfaces are indicative of the intergrannular cleavage fracture mechanism. Therefore, the fracture mechanism in this aging condition is a mixture of classical ductile fracture and to a lesser extent, cleavage fracture. The EDX analysis showed

that cracked area contained high amount of Si; in the A357 alloy, high quantities of Si are observed only in the Si particles that they are preferably located in-between the dendrites. This observation is also an indication of an intergrannular fracture mode.

For the overaged specimen no signs of smooth surfaces were observed but only rough surfaces consisting of large dimples and cavities. For the overaging condition in A357 alloys, the strengthening phase begin to coarsen and, to a lesser extent, the Si particles are rounded. This means that the phases in the microstructure of the alloy with high aspect ratio become more spherical and they do not behave as stress raisers. As a consequence, the nucleation of micro-cracks in the matrix is suppressed that enhances ductility. Hence, the governing fracture mode for this case is the classical ductile rupture.

5.2 Modifications in chemical composition

The microstructure of the Cu-modified alloy was not refined when compared to the reference A357 alloy. This was mainly attributed to the negative influence of the addition of Cu to the eutectic structure. As already mentioned earlier, the copper addition favored an acicular structure of the silicon particles, Figure 9. This Si geometry acts as a stress raiser in the aluminum matrix, thus resulting in a loss of the ductility of the matrix. Therefore, the resulting microstructure of the Cu-modified alloy can explain that the 4% increase in strength is due to precipitation of the θ'' phase, as well as the 56% decrease in ductility is due to the more acicular structure of the Si particles.

As the fracture toughness is dominated by both, strength and ductility properties, a logical argument cannot be made. Nevertheless, by the great decrease of 56% in ductility

and the minor increase of 4% in strength one can suspect that a decrease in the fracture toughness of the Cu-modified alloy should occur. Indeed, K_{Ic} was decreased by almost 15% when compared to the reference alloy.

The addition of the other minor elements such as Ag and Sm to the Cu-modified alloy didn't decrease the size of the Si particles nor its morphology. On the contrary, it was shown that the Si size of the alloy further coarsen and its morphology was more fibrous, Figure 9. Hence, this is evidence that the alloys with the above elements should present lower ductility values than the Cu-modified alloy. The decrease in ductility was of the order of 5% for the Ag modified alloy up to 50% for the Ag+Sm modified alloy, Table 3.

It is well known that the addition of Sr to A357 modifies the Si particles to a more rounded morphology [34]. As can be seen in the literature alloys, both, ductility as well as fracture toughness is enhanced by the Sr modification. For the experimental alloys, the resulting globular Si morphology increased by almost 50% the ductility of the material, when compared to the Cu-modified alloy.

5.3 Elongation to fracture - strain energy density

It is reported in the literature that the elongation to fracture A_f is analogous to the tensile toughness (strain energy density) W for the case of ductile materials [42, 43]. In this work, a direct correlation of these two - fracture related - properties is attempted for all artificial aging conditions as well as for the different chemical modifications of the A357 cast aluminum alloy. The results are presented in Figures 12(a) and (b), respectively, which suggest a linear relationship. A linear approximation is confirmed for all the available test results ($R^2 = 0.98$

and 0.99, respectively). Nevertheless, the slope of the correlation between the two material properties changes from foundry to foundry, probably due to different solidification rate of the castings. Similar observations were made previously [44] for A357 alloy aerospace castings.

An approximation to eqn.(6) can be made [45, 46] as:

$$W \simeq \left(\frac{R_p + R_m}{2}\right) \cdot A_f. \tag{15}$$

The use of the above equation is enhanced to calculate the strain energy density values of cast alloys from material databases. Nevertheless, the calculation error increases for the alloys that present high values of the ratio $\frac{R_m}{R_p}$ [32]. In the same work, analytical expressions have been provided and discussed for the more accurate calculation of the strain energy density values of a cast alloy from the above tensile mechanical properties.

5.4 Strain energy density - strain-hardening exponent

Many scientists, e.g. [16], used the strain-hardening exponent n as a measure of the energy absorption during the tensile test of a material. Nevertheless, to the authors' knowledge a direct correlation between the strain-hardening exponent and strain energy density has not been established in the literature. An approximation can be made by using the Ludwik-Hollomon equation, where the engineering stress-strain curve can be obtained from equation (2), by ignoring the elastic component of the strain and assuming volume is preserved and

the material deforms uniformly until final failure. Hence, equation (2) becomes:

$$\sigma = H \cdot \frac{[ln(1+\varepsilon)]^n}{(1+\varepsilon)}. \tag{16}$$

At the value of ultimate strength R_m, the slope of the flow curve is zero. By differentiating equation (16) it follows:

$$n = ln(1 + A_g), \tag{17}$$

where A_g is the uniform elongation (engineering strain at R_m) of the alloy. Equation (16) for $\sigma = R_m$ and $\varepsilon = A_g$, gives:

$$H = \frac{R_m \cdot (1 + A_g)}{n^n}. \tag{18}$$

The strain energy density W can be calculated as the integral of the engineering flow curve of equation (16), from $\varepsilon = 0$ to $\varepsilon = A$, where A is the engineering strain at fracture. When combining equations (16), (17) and (18), the W can be calculated as an expression of:

$$W_{In} \approx W = \int_0^A \sigma \cdot d\varepsilon = \frac{R_m \cdot e^n \cdot \ln^{n+1}(1 + A)}{n^n \cdot (n + 1)}. \tag{19}$$

The results of the approximate expression of the strain energy density W_{In} are plotted in Figure 13 over the strain energy density W values of the experiments. The proposed approximation provides respectable estimates, and thus the strain energy density is actually a function of the properties n, A and R_m. For all alloys investigated in this work, the strain energy density values can be estimated by the following expression and as a sole function of

the strain-hardening exponent n and elongation at fracture A, as:

$$W_n \approx W = \left(\sqrt{n \cdot A}\right) \cdot R_m. \tag{20}$$

Figure 13 depicts the very good correlation results ($R^2 = 0.98$) between the evaluated strain energy density property and the calculated $W_n = \left(\sqrt{n \cdot A}\right) \cdot R_m$ values. The direct correlation is valid, since the strain-hardening exponent actually reflects the ability of the alloy to re-direct the plastic strain in the material's microstructure and hence, should be considered as a measure for the tensile energy capacity of the material.

5.5 Fracture toughness and strain-hardening exponent

The mechanical properties reported for A357 alloy in another study [4] has been also used in the present work for comparison purposes. The mechanical properties of for this alloy can be seen in Table 3. This A357 was produced with or without Sr modification (designated as (M) and (UM), respectively) and was heat treated to T4 and T61 conditions. For all four cases, their material properties W, n and H were estimated by using analytical equations presented in [32].

The artificial aging of the 20 h at 155°C of the A357 alloy of the present study, aimed to bring the alloy into the underaging condition and just before its peak-strength condition (T6). Hence, it is expected that fracture toughness K_{Ic} should vary between these two values. Indeed the experimental value of 28.9 MPa$\cdot\sqrt{m}$ of A357 is amongst the values of 30.4 for the unmodified A357 of T4 condition and the 21.2 MPa$\cdot\sqrt{m}$ of the T61 condition of

the literature alloy. Thus, the experimentally derived value is in good agreement with the literature.

Following the empirical correlation between K_{Ic} and n of equation (4), the data developed in the present work have been plotted in Figure 14, which shows that the equation suggested by Tagami et al [23] does not provide a good fit to the experimental data. The empirical constant B of equation (4) has been calculated for all investigated cast alloys and are shown additionally in Figure 14. The empirical constant B varies from the value of 20.84 $(\text{MPa}\cdot\text{m})^{1/2}$ for the A357 alloy up to the value of 78.13 $(\text{MPa}\cdot\text{m})^{1/2}$ for the A357+1% Cu+Ag+Sm alloy. These values are by far away from the values of the literature, e.g. 13.1 $(\text{MPa}\cdot\text{m})^{1/2}$ reported in [23] or the value of 17.66 $(\text{MPa}\cdot\text{m})^{1/2}$ reported in [25].

The linear approximation between fracture toughness K_{Ic} and the term $n \cdot \sqrt{R_p}$ values proposed in Figure 14, provides a better fit to the experimental data in this work. Hence the revised Hahn-Rosenfield equation introduced by Tagami et al. can be modified as a linear expression of the form:

$$K_{Ic} = c \cdot \left(n \cdot \sqrt{R_p}\right) + d, \tag{21}$$

where $c = 5.56$ $(\text{MPa}\cdot\text{m})^{1/2}$ and $d = 21.71$ $\text{MPa}\sqrt{m}$ are empirical derived coefficients for A357. The physical meaning of the empirical constant d can be interpreted as the 'principial' fracture toughness value of the specific alloy. This value of 'principial' fracture toughness is a function of the solidification rate and chemical composition of the material. The coefficient c has the same units with the coefficient B in the equation (4), and hence it represents the increase of the fracture toughness with the increase of the yield strength and plasticity of the material. Further research is needed to test the validity of the empirical equation (21).

The experimental data were plotted in Figure 15 in the form as proposed by Peel et al.: $\frac{K_{Ic}^2 \cdot (1-\nu^2)}{E}$ versus $\frac{H \cdot \varepsilon_f^{1+n}}{1+n}$. Despite the simplicity of the fracture model to estimate fracture toughness, the equation proposed by Peel et al. indicate how the two parameters involved control the fracture toughness. The first is the plastic zone size r and the second is the plastic deformation characteristics governed by ε_f, H and n. Note that the latter characteristics have a strong influence on the strain energy density W (tensile toughness). Thus, this is further indication that the fracture toughness is related to the tensile toughness.

The data fall on a straight line as can be seen in Figure 15. The slope of the line equals to $2 \cdot r$, according to equation (9), thus giving value of 122.58 μm, or an average value of $r = 61.29$ μm for the investigated alloys. It is apparent that all the alloys possess the same plastic zone size r values; the r value is dependent upon solidification conditions, modification, chemical composition and temper. The experimental data verify ($R^2 = 0.91$) the fracture model of Peel et al. in the respective Figure, thus providing an easy method to estimate plane strain fracture toughness.

5.6 Fracture toughness and strain energy density

It has been shown in equation (13) that there is a relationship between K_{Ic}^2 and the strain energy density W values of a ductile material. The experimental data have been plotted in Figure 16 which shows that there is wide scatter. However a linear relationship can be written with a fairly good approximation ($R^2 = 0.91$). The data for K_{Ic}^2 and W can be substituted to equation (13) to calculate the critical ligament r_c from the crack tip for each alloy, assuming that that the Poisson ratio ν is constant. The calculation results can also

be found in the same Figure. The calculated ligaments ranged from 26 to 83 μm for the investigated alloys. The high calculated ligament size of both alloys A357+1% Cu+Sm and A357+1% Cu+Ag+Sm was attributed to both, medium fracture toughness and low strain energy density values of the respective alloys (Figure 10). Nevertheless, it is the authors' opinion that the average ligament size should yield to a fixed value around 30 to 40 μm. This ligament size r_c of the same order of magnitude to the DAS for each alloy, as measured in the framework of the project ADVACAST [5].

A further simplification to correlate the tensile and fracture toughness values of the alloys is proposed in Figure 17. The test data were directly correlated by the linear expression:

$$K_{Ic} = f \cdot W + g, \tag{22}$$

where $f = 0.2705\ \sqrt{m}$ and $g = 21.36\ \text{MPa}\sqrt{m}$ are empirically derived constants. The standard deviation of equation (22) remains the same ($R^2 = 0.91$) as of equation proposed in Figure 16. Please also note that the empirical coefficient d in equation (21) and g in equation (22) have almost identical values. This further supports the concept of the 'principial' fracture toughness of a brittle alloy that fractures without any plasticity. The higher the plasticity capacity of an alloy (which is expressed in terms of W in the specific equation), the higher fracture toughness value will present.

A more accurate expression to correlate the fracture-related properties can be reached by using the empirical equation suggested by Barson and Rolfe (14). When substituting the impact energy W_{CVN} values by the strain energy density W values, equation (14) takes the

form:

$$\left(\frac{K_{Ic}}{R_p}\right)^2 = p \cdot \left(\frac{W}{R_p}\right)^2 + q. \tag{23}$$

The plot of the pairs of the terms $\left(\frac{K_{Ic}}{R_p}\right)^2$ and $\left(\frac{W}{R_p}\right)^2$ for the investigated cast aluminum alloys can be seen in Figure 18. A linear expression can fit the pairs of the above terms and the empirical coefficients of equation (23) take values $p = 0.871$ m and $q = 0.004$ m. The fit is quite impressive as evidenced by the high R^2 of 0.98. This equation can provide a reliable estimate of the fracture toughness of A357 alloy, given their tensile properties R_p, and W. The validity of equation (23) for cast aluminum alloys with different solidification rates or from other aluminum alloys should be determined by further research.

6 Conclusions

- With increasing artificial aging time, strain-hardening coefficient decreases linearly with yield strength down to the minimum value of 0.05 for the peak-aged condition. With over-aging, the strain hardening exponent increases with decreasing yield strength.

- Analysis of the fracture surfaces indicated that the fracture mechanism is consistent to the aging condition of the material; both ductile fracture as well as to a lesser extend, quasi-cleavage fracture were observed in the investigated cases.

- Minor alloying additions of Cu, as well as Ag and Sm to the A357 alloy resulted in a marginal increase in strength, possibly due to the precipitation of the θ'' phase during artificial aging. Nevertheless, all the additions coarsen the Si particles and they were formed in a more acicular (fibrous) morphology than those in the reference A357 alloy. This structure resulted in a significant loss in ductility.

- The addition of 1% Cu in the A357 alloy resulted in 4% increase in strength and almost 56% decrease in ductility. As the fracture toughness is dominated by both, strength and ductility properties, the 15% decrease in fracture toughness K_{Ic} can be judged as a fair result.

- The minor additions of Ag and Sm in the Cu-modified alloy didn't altered the fibrous microstructure of the Si particles, and hence, no increase in ductility nor in fracture toughness was observed.

- Strain energy density and elongation to fracture have a strong linear relationship, while an analogy to the $\sqrt{n \cdot A}$ values was also observed for the investigated alloys.

- A linear relationship between fracture toughness and strain energy density was observed; the concept of principial fracture toughness of an alloy is discussed.

- Empirical relationships to estimate plane strain fracture toughness from the tensile properties including strain-hardening exponent, yield strength and strain energy density have been developed. These relationships were found to provide good estimates for the A357 alloy.

2

References

[1] M. Tiryakioğlu, J. Campbell, and J.T. Staley. The influence of structural integrity on the tensile deformation of cast Al-7wt.%Si-0.6wt.%Mg alloys. *Scripta Materialia*, 49(9):873–878, 2003.

[2] C. Nyahumwa, N.R. Green, and J. Campbell. Influence of casting technique and hot isostatic pressing on the fatigue of an Al-7Si-Mg alloy. *Metallurgical and Materials Transanctions A*, 32A(2):349–358, 2001.

[3] S.K. Koh and R.I. Stephens. Fracture toughness of A357-T6 cast aluminum alloy. *SAE-SP760*, Fatigue and fracture toughness of A357-T6 cast aluminum alloy:61–69, 1988.

[4] D.A. Lados and D. Apelian. Fatigue crack growth characteristics in cast Al-Si-Mg alloys Part I: Effect of processing conditions and microstructure. *Materials Science and Engineering A*, A385(1):200–211, 2004.

[5] Anon. Advanced Aluminum Precision Casting For Integrally Stiffened Net - Shape Components (ADVACAST). Final Technical Report of the BRITE Project 4084, Brussels, Belgium, 1996.

[6] N.D. Alexopoulos. Development of new near net shape cast aluminum alloys with improved mechanical properties. Final Technical Report of the Project YPER 94/274, Greek General Secreriat of Research and Technology, Patra, Greece (in Greek), 2002.

[7] Anon. Production and development of cast aluminum components for aeronautical applications. Final Technical Report of the Project PABE 96BE/219, Greek General Secreriat of Research and Technology, Bolos, Greece, (in Greek), 2000.

[8] D. Granger and M. Kersker. Effect of beryllium on the properties of A357.0 castings. *AFS Transactions*, 115:579–586, 1984.

[9] M. Misra and K. Oswalt. Aging characteristics of titanium-refined A356 and A357 aluminum castings. *AFS Transactions*, 70:1–10, 1982.

[10] O. Vorren, J. Evensen, and T. Pedersen. Microstructure and mechanical properties of Al-Si-Mg casting alloys. *AFS Transactions*, 162:459–466, 1984.

[11] G. Nagel and R. Portalier. Structural modification of Aluminum - Silicon alloys by antimony treatment. *AFS International Cast Metals Journal*, 34:2–6, 1980.

[12] S. Murali, K. Raman, and K. Murthy. Effect of magnesium, iron (impurity) and solidification rates on the fracture toughness of Al-7Si-0.3Mg casting alloy. *Materials Science and Engineering A*, A151:1–10, 1992.

[13] Y.H. Tan, S.L. Lee, and Y.L. Lin. Effects of Be and Fe content on the microstructure and mechanical properties of A357.0 alloys. *Metallurgical and Materials Transactions A*, 26A:1195–1205, 1995.

[14] L. Qiyang, L. Qingchun, and L. Qifu. Modification of Al-Si alloys with sodium. *Acta Metallurgica Materialia*, 39(11):2497–2502, 1991.

[15] N.D. Alexopoulos and Sp.G. Pantelakis. Evaluation of the effects of variations in chemical composition on the quality of Al-Si-Mg, Al-Cu and Al-Zn-Mg cast aluminum alloys. *J. of Materials Engineering and Performance*, 12(2):196–205, 2003.

[16] G.T. Hahn and A.R. Rosenfield. Sources of fracture toughness: The relationship between K_{Ic} and the ordinary tensile properties of metals. In *Applications Related Phenomena in Titanium Alloys*, pages 5–32. ASTM STP 432, 1968.

[17] J. Barson and S. Rolfe. Correlations between K_{Ic} and Charpy V-notch test results in the transition-temperature range. In *Impact Testing of Metals*, pages 281–302. ASTM STP 466, 1970.

[18] J.T. Staley. Microstructure and toughness of high-strength aluminum alloys. In *Properties Related to Fracture Toughness*, pages 71–103. ASTM STP 605, 1976.

[19] G.T. Hahn and A.R. Rosenfield. Metallurgical factors affecting fracture toughness of aluminum alloys. *Metallurgical Transactions A*, 6A:653–668, April 1975.

[20] K.V. Jata and E.A. Starke Jr. Fatigue crack growth and fracture toughness behaviour of an Al-Li-Cu alloy. *Metallurgical Transactions A*, 17A:1011–1026, 1986.

[21] J. R. Davis, editor. *ASM Specialty Handbook: Aluminum and Aluminum Alloys*. ASM International, Metals Park, Ohaio, USA, 1993.

[22] N. Kamp, I. Sinclair, and M.J. Starink. Toughness - strength relations in the overaged 7449 Al-based alloy. *Metallurgical and Materials Transanctions A*, 33A:1125–1136, 2002.

[23] M. Tagami, Y. Serita, and T. Tokita. Fracture toughness of Al-10%Si -3%Cu -0.3%Mg die castings. *Journal of Japan Institute of Light Metals*, 30(11):648–652, 1980.

[24] M. Tagami and Y. Serita. Fracture toughness of Al-7%Si-0.5%Mg alloy castings. *Journal of Japan Institute of Light Metals*, 30(7):390–393, 1980.

[25] G. Terjesen. Qualitatskriterien fur die bruchzahigkeit von Al-Si-10Mg gusslegierungen. *Aluminium*, 78(12):1088–1093, 2002.

[26] C.J. Peel and P.J.E. Forsyth. The effect of composition changes on the fracture toughness of an Al-Zn-Mg-Cu-Mn forging alloy. *Metal Science Journal*, 7:121–127, 1973.

[27] D. Yeong, O. Orringen, and G Sih. Strain energy density approach to stable crack extension under net section yielding of aircraft fuselage. *J. Theoretical and Applied Fracture Mechanics*, 22:127–137, 1995.

[28] G. Sih and C. Chao. Failure initiation in unnotched specimens subjected to monotonic and loading. *J. Theoretical and Applied Fracture Mechanics*, 2:67–73, 1984.

[29] G. Sih and D. Yeong. Fatigue load sequence effect ranked by critical available energy density. *J. Theoretical and Applied Fracture Mechanics*, 14:141–151, 1990.

[30] D. Apelian, S. Shivkumar, and G. Sigworth. Fundamental aspects of heat treatment of cast Al-Si-Mg alloys. *AFS Trans.*, 137:727–742, 1989.

[31] N.D. Alexopoulos and Sp.G. Pantelakis. Quality evaluation of A357 cast aluminum alloy specimens subjected to different artificial aging treatment. *Materials & Design*, 25:419–430, 2004.

[32] N.D. Alexopoulos and Sp.G. Pantelakis. Quality assessment of artificially aged A357 aluminum alloy cast ingots by introducing approximate expressions of the quality index Q_D. *Metallurgical and Materials Transanctions A*, 35A(10):3079–3089, 2004.

[33] M. Tiryakioğlu and N.D. Alexopoulos. The effect of artificial aging on tensile work hardening characteristics of a cast Al-7%Si-0.55%Mg (A357) alloy. *Metallurgical and Materials Transanctions A*, 39A:2772–2780, 2008.

[34] R. DasGupta, Brown C., and S. Marek. Analysis of strontium - modified A356 aluminum alloy. In T. Khan and G. Effenberg, editors, *Advanced Aluminum and Magnesium Alloys*, pages 501–508. International Conference on Light Metals, ASM International, Amsterdam, 1990.

[35] J. Gurland and J. Plateau. The mechanism of ductile rupture of metals containing inclusions. *ASM Transactions*, 56:42–454, 1963.

[36] A. Gangulee and J. Gurland. On the fracture of Si particles in Al-Si alloys. *Trans. Met. Soc. of AIME*, 239:269–280, 1967.

[37] R. Doglione, J. Douziech, C. Berdin, and D. Francois. Microstructure and damage mechanisms in A356-T6 alloy. *Mater. Sci. Forum*, 217-222:1435–1440, 1996.

[38] C. Meyers and J. Chou. Experimental investigations of deformation in HIPped A356 aluminum castings. *AFS Transactions*, 99:775–786, 1991.

[39] L. Zhen and S.B. Kang. Deformation and fracture behavior of two Al-Mg-Si alloys. *Metallurgical and Materials Transanctions A*, 28A:1489–1497, 1997.

[40] Q.G Wang and C.H. Caceres. The fracture mode in Al-Si-Mg casting alloys. *Materials Science and Engineering A*, A241:72–82, 1998.

[41] Y.H. Tan, S.L. Lee, and Y.L. Lin. Effects of Be and Fe content on plane strain fracture toughness in A357 alloys. *Metallurgical and Materials Transactions A*, 26A:2937–2945, 1995.

[42] M. Tiryakioğlu, J.T. Staley, and J. Campbell. Evaluating structural integrity of cast Al-7%Si-Mg alloys via work hardening characteristics II. A new quality index. *Materials Science and Engineering A*, A368:231–238, 2004.

[43] M. Tiryakioğlu, J.T. Staley, and J. Campbell. *Materials Science and Engineering A*, A487:383–387, 2008.

[44] M. Tiryakioğlu and J. Campbell. Evaluation of structural integrity in cast Al-7%Si-Mg alloys via toughness. In *Mechanisms and Mechanics of Fracture: Symposium in Honor of Prof. J.F. Knott*, pages 111–115. TMS, Columbus, Ohio, Oct 2002.

[45] N. Dowling. *Mechanical Behavior of Materials*. Prentice Hall, New Jersey, USA, 2nd edition, 1993.

[46] G.E. Dieter. *Mechanical Metallurgy*. Mc-Graw-Hill, third edition, 1986.

List of Figures

35

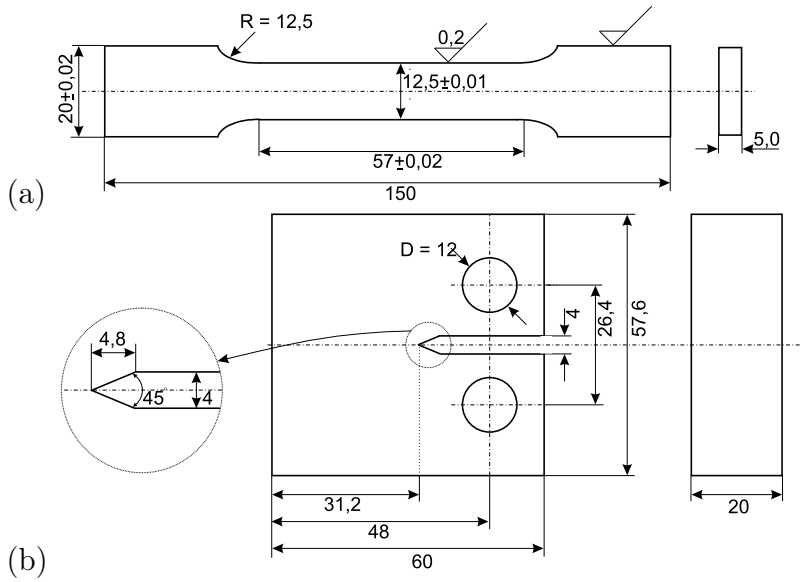

Figure 1: (a) Tensile and (b) fracture toughness test specimen configurations of the investigated aluminum alloy according to the specifications ASTM E8 and E399, respectively.

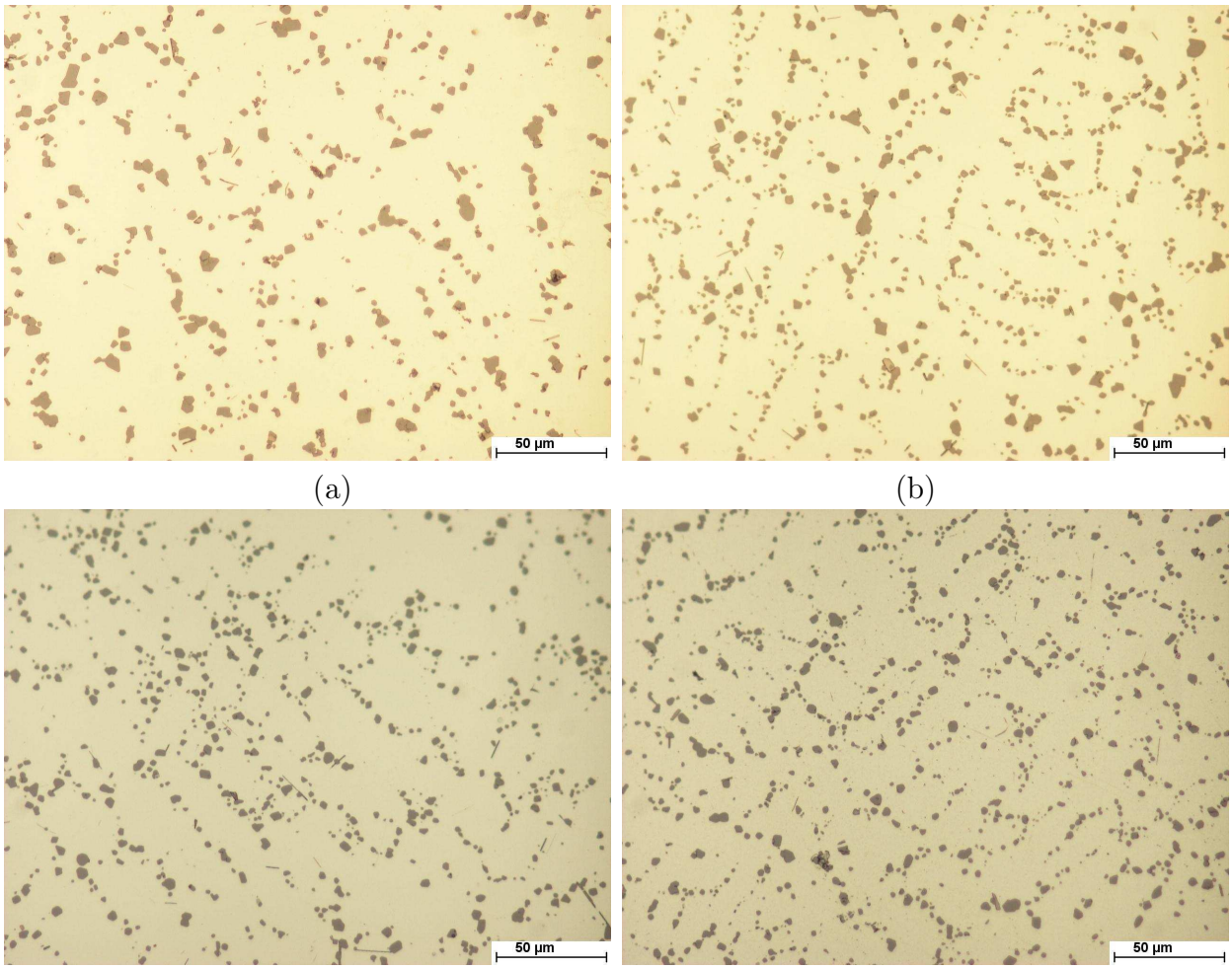

(a) (b)

(c) (d)

Figure 2: Typical microstructures of the A357 cast aluminum alloy for different heat treatment artificial aging conditions: (a) solid solution, (b) 12 hours at 155°C, (c) 48 hours at 175°C, and (d) 36 hours at 205°C.

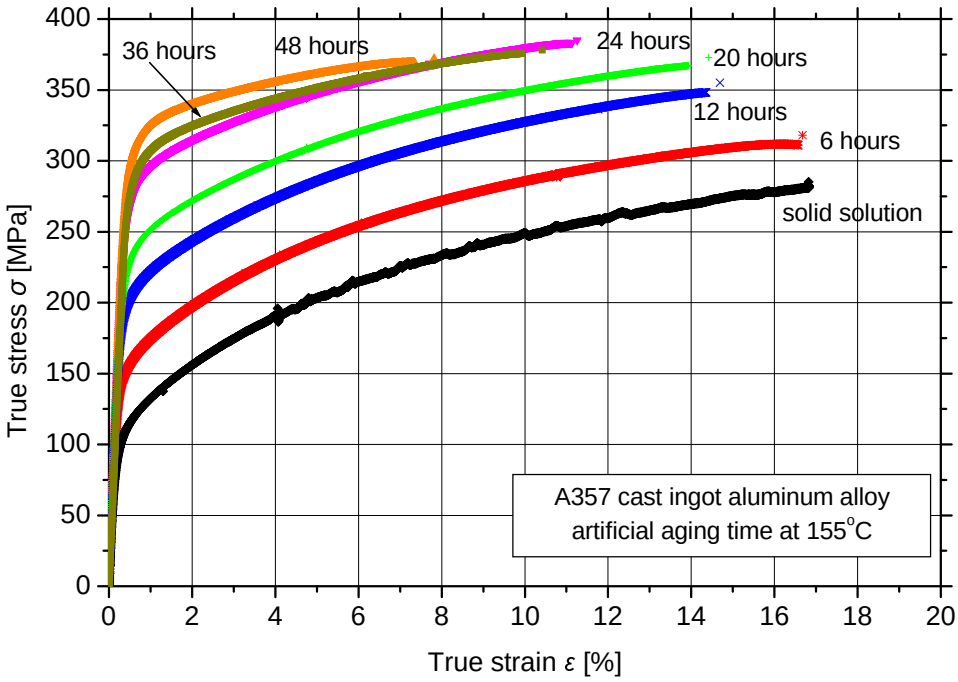

Figure 3: Typical true stress - true strain tensile flow curves of the A357 cast aluminum alloy for different artificial aging heat treatment conditions.

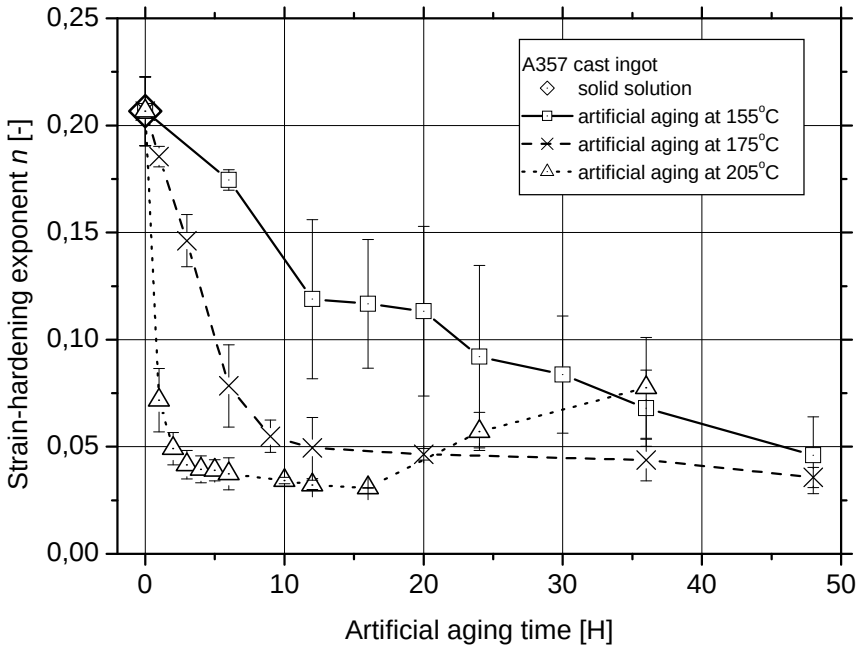

Figure 4: Strain-hardening exponent n for the different artificial aging heat treatment conditions of the A357 cast aluminum alloy.

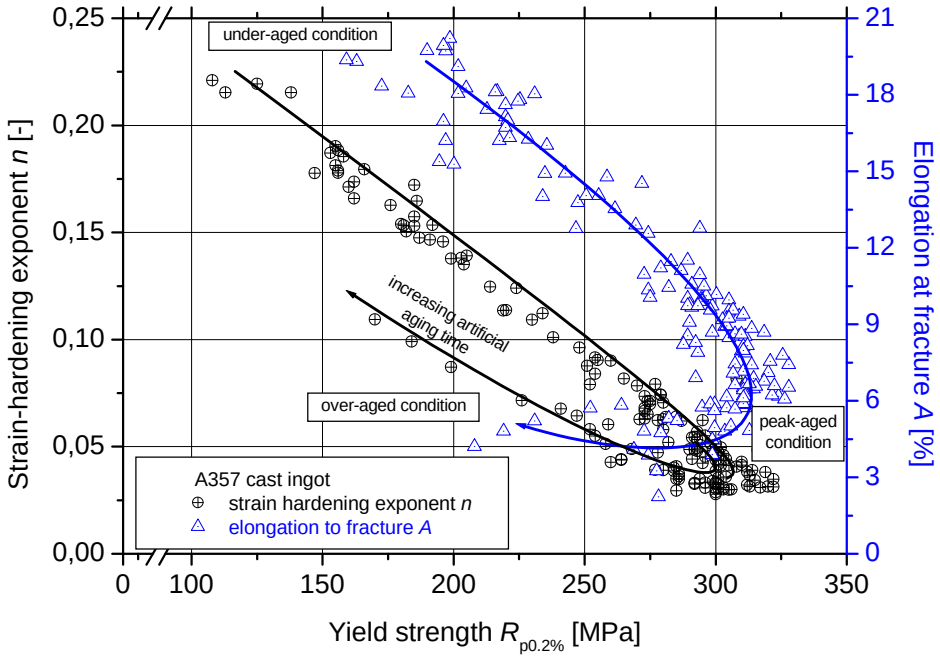

Figure 5: Strain-hardening exponent n and elongation at fracture A values versus the yield strength R_p values for the different artificial aging heat treatment conditions of the A357 cast aluminum alloy.

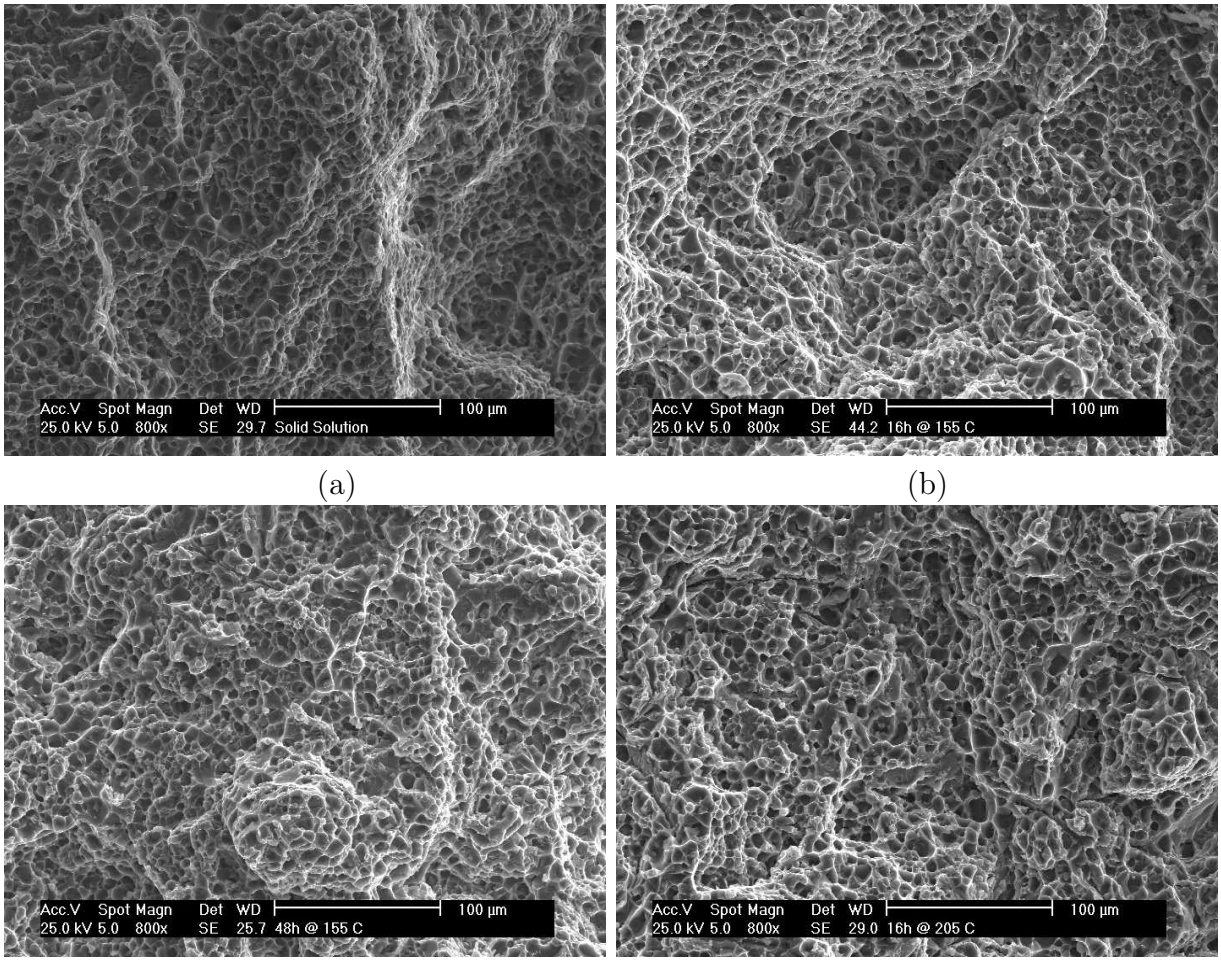

Figure 6: SEM images of the fracture surfaces of the tensile specimens of the A357 cast aluminum alloy for different heat treatment artificial aging conditions: (a) solid solution, (b) 16 hours at 155°C, (c) 48 hours at 155°C, and (d) 16 hours at 205°C.

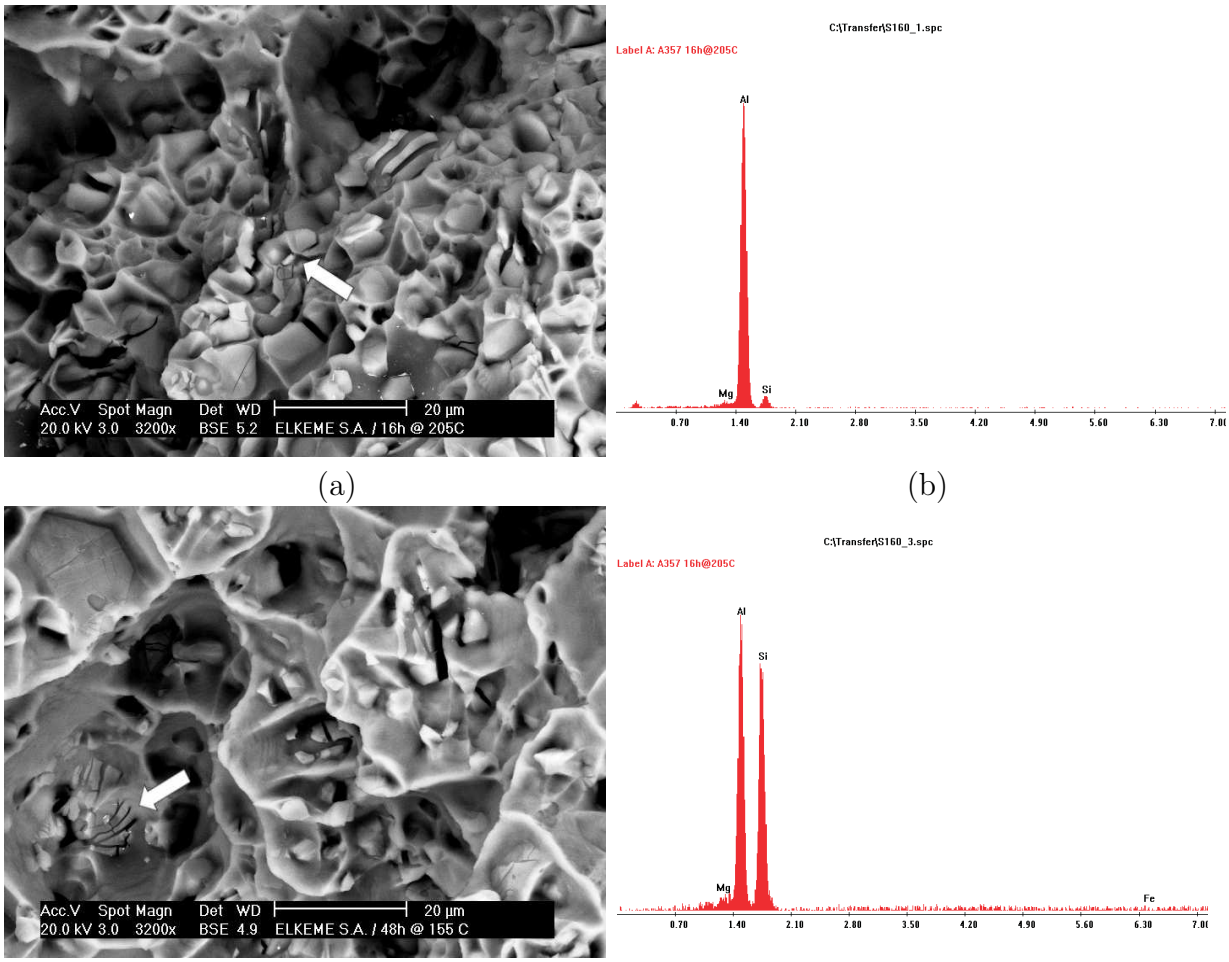

Figure 7: SEM images of the fracture surfaces of the tensile specimens of the A357 cast aluminum alloy for heat treatment artificial aging conditions of (a) 16 hours at 205°C and (b) chemical analysis of the indication and (c) 48 hours at 155°C and (d) chemical analysis of the indication point.

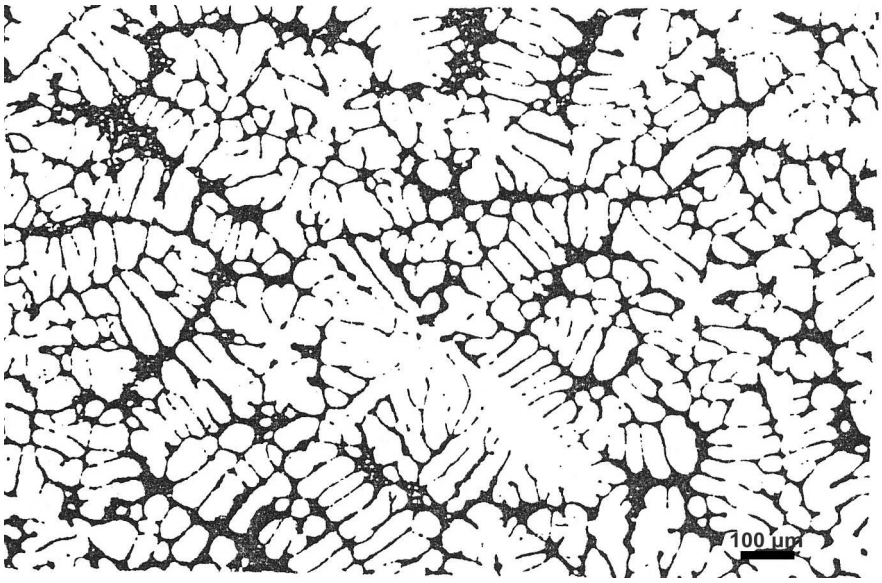

Figure 8: Microstrusture of the alloy A357 produced with the SOPHIA process in the as-cast condition.

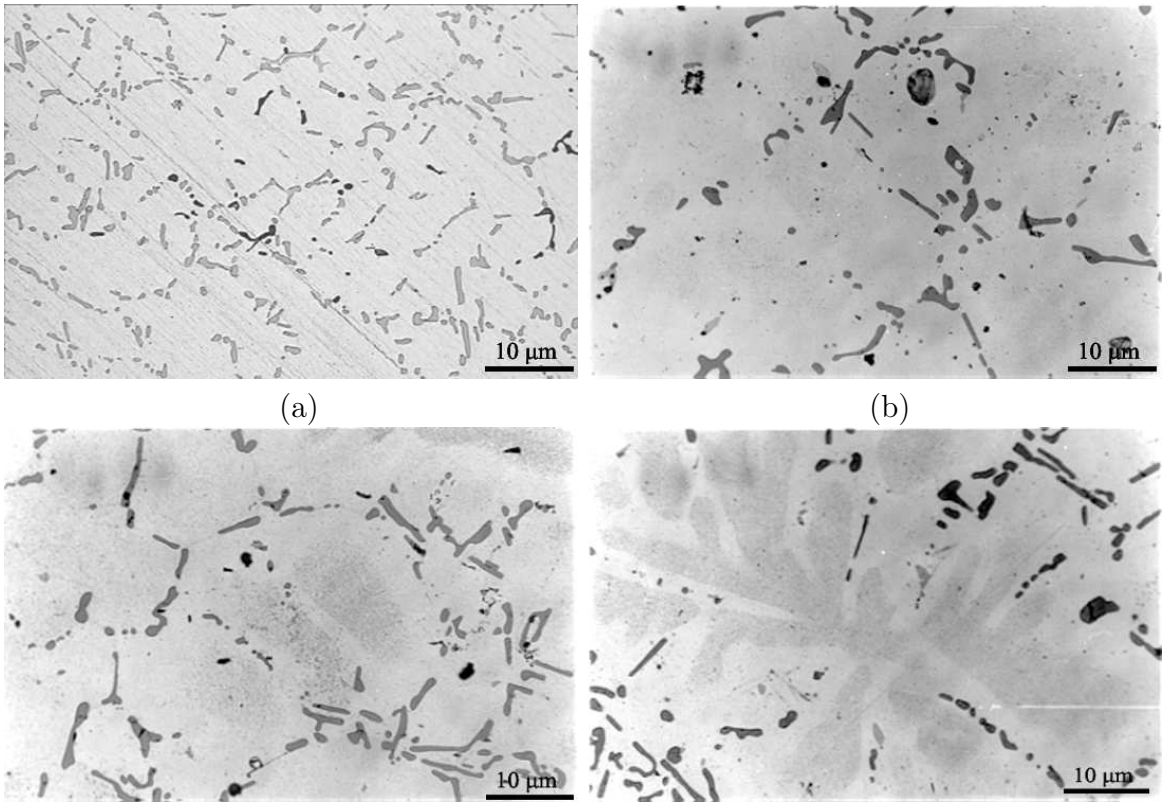

(a) (b)

(c) (d)

Figure 9: Typical microstructures of the SOPHIA cast aluminum alloys: (a) A357, (b) A357 + 1% Cu, (c) A357 + 1% Cu + Ag, and (d) A357 + 1% Cu + Sm.

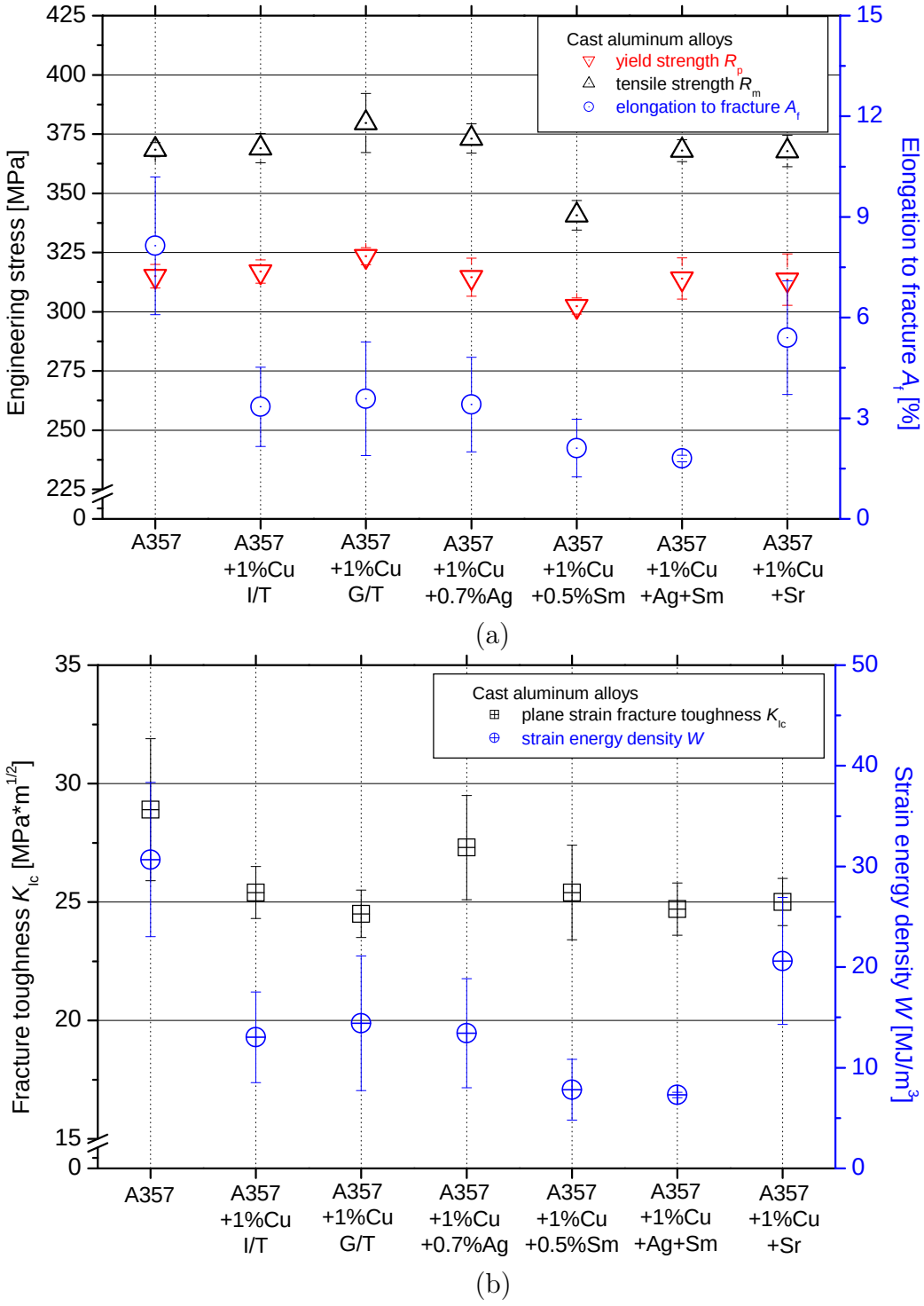

Figure 10: (a) Yield strength R_p, tensile strength R_m and elongation to fracture A_f and (b) fracture toughness K_{Ic} and strain energy density W values of the investigated cast aluminum alloys.

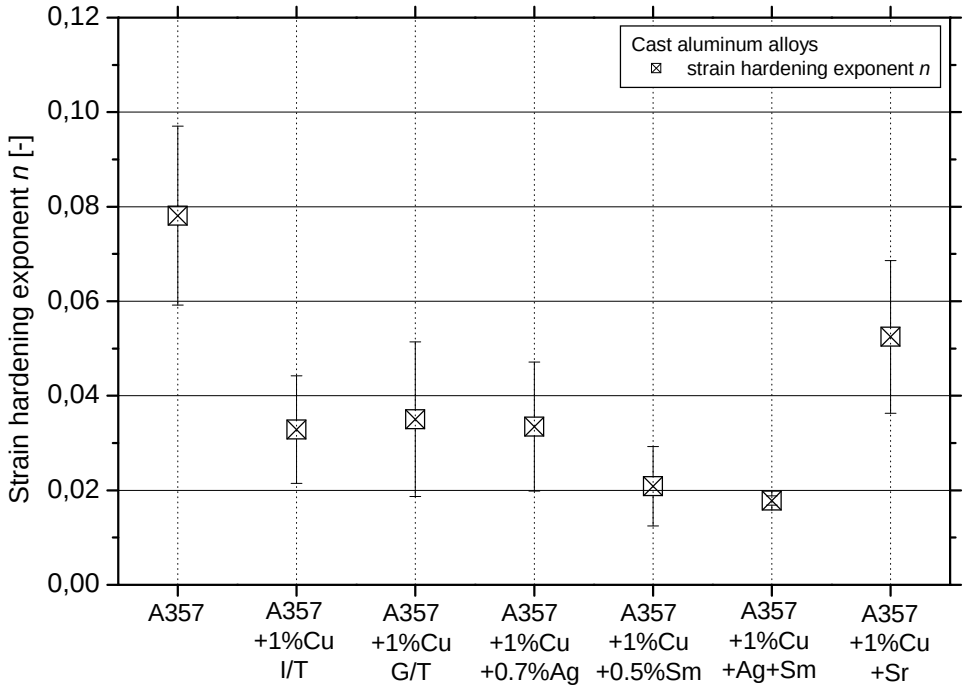

Figure 11: Strain-hardening exponent values n of the investigated A357 cast aluminum alloys with minor chemical modifications.

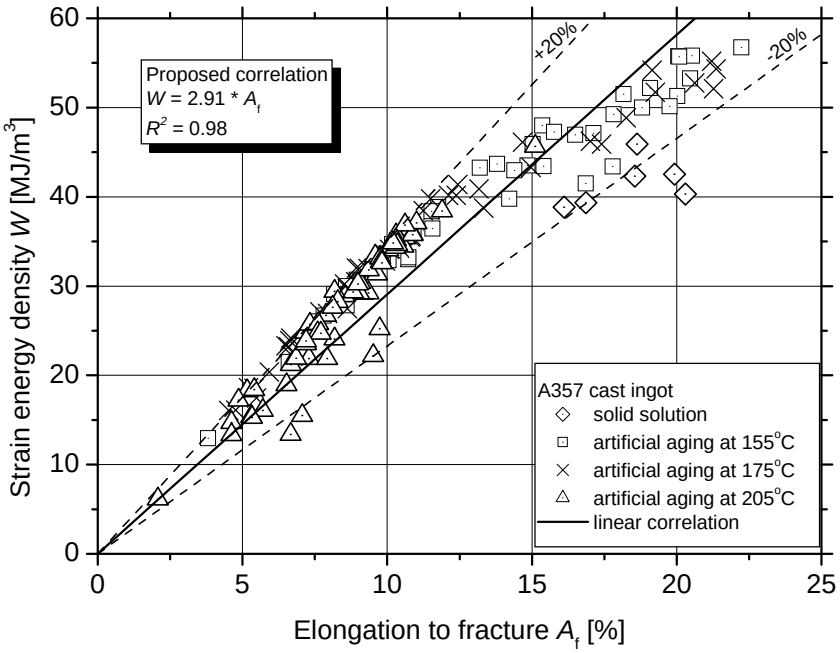

(a)

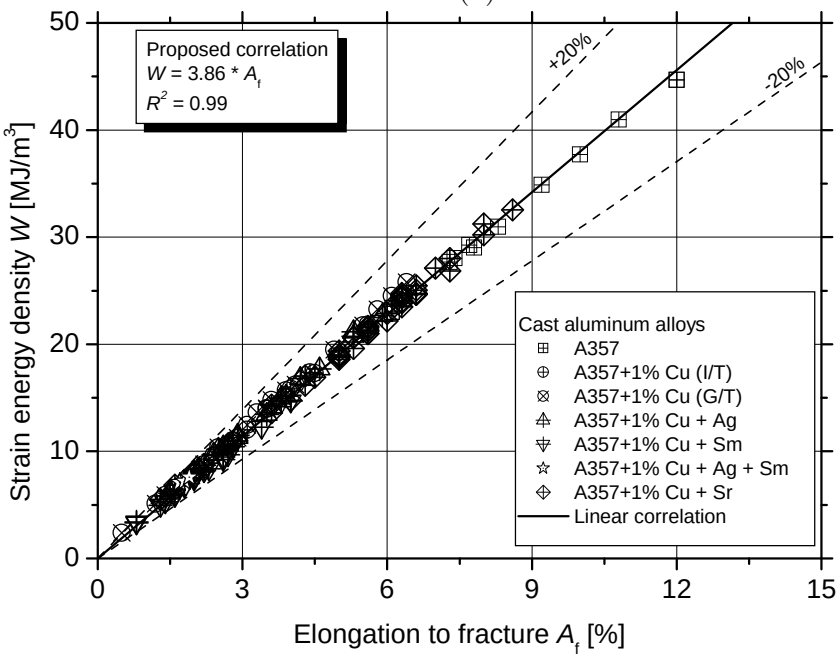

(b)

Figure 12: Correlation between strain energy density W and elongation to fracture A_f values for the investigated A357 alloys for (a) different artificial aging heat treatment conditions and (b) minor chemical modifications.

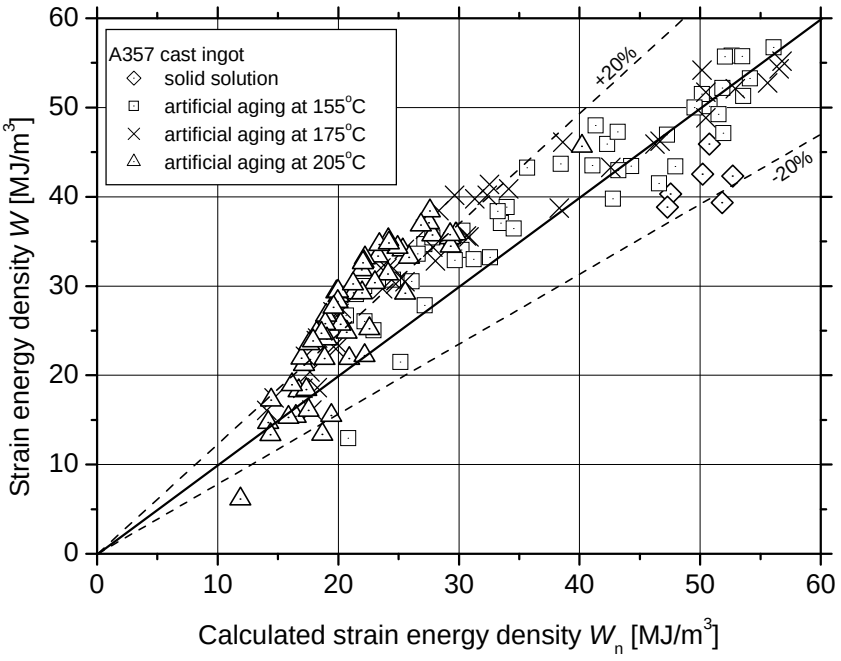

(a)

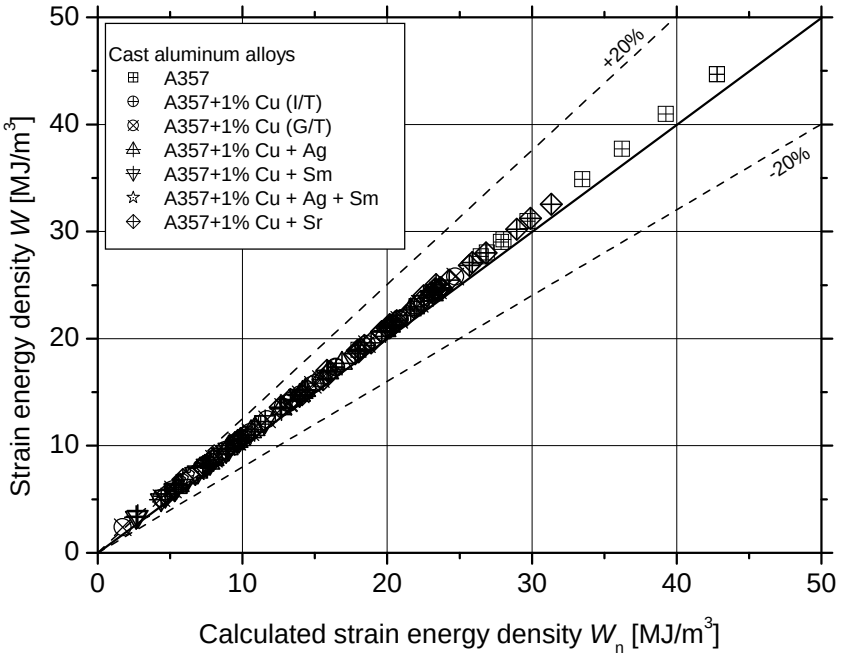

(b)

Figure 13: Correlation between strain energy density W and $W_n = \left(\sqrt{n \cdot A}\right) \cdot R_m$ values for the investigated A357 alloys for (a) different artificial aging heat treatment conditions and (b) minor chemical modifications.

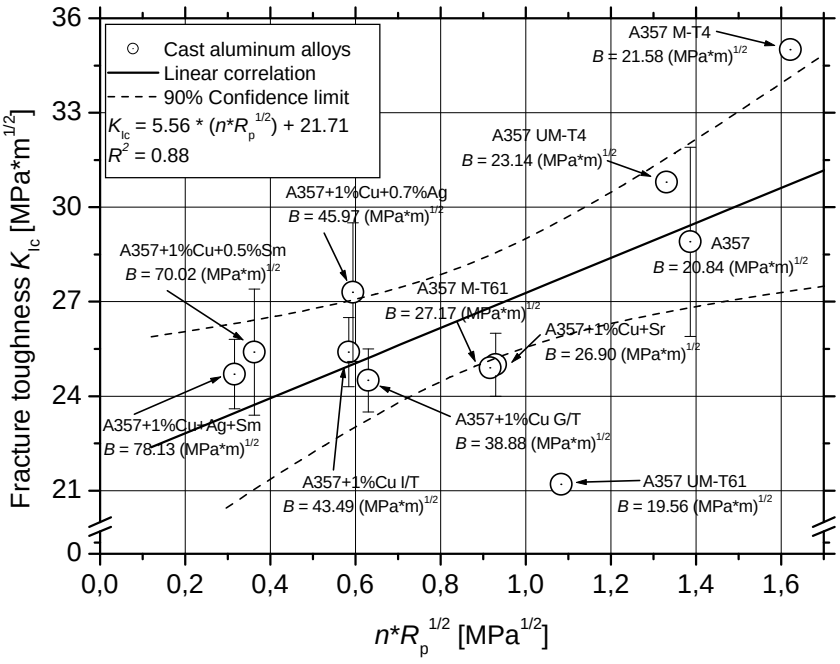

Figure 14: Correlation between fracture toughness K_{Ic} and strain-hardening exponent n values.

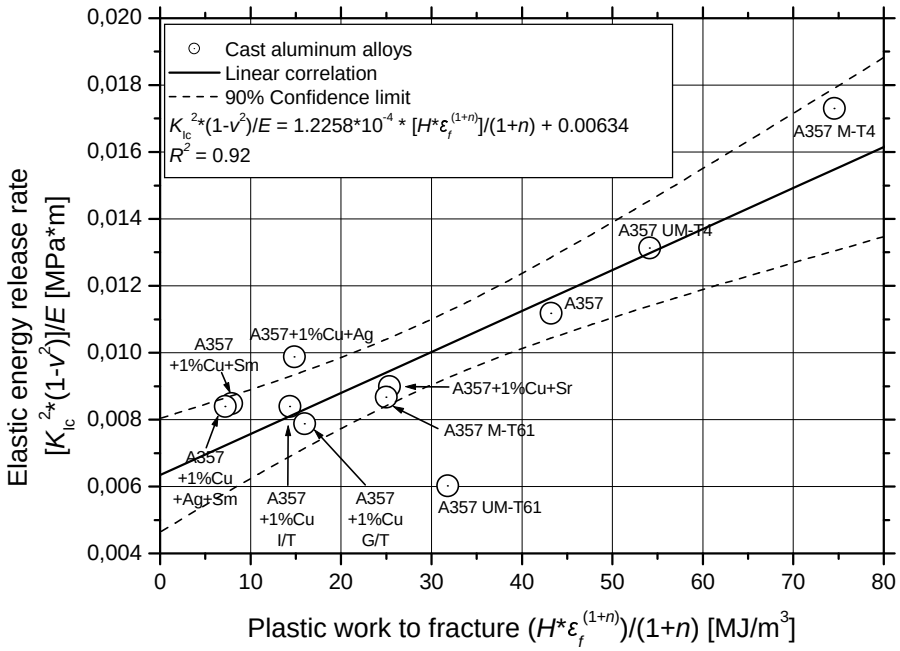

Figure 15: Correlation between fracture toughness K_{Ic} and strain-hardening exponent n values.

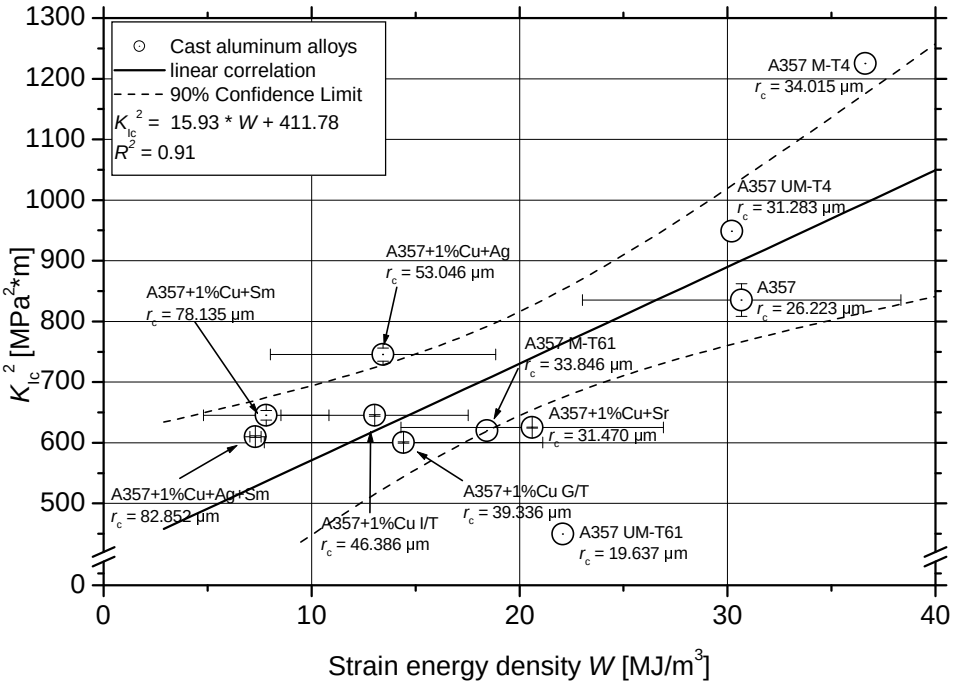

Figure 16: Correlation between strain energy density W and square of fracture toughness K_{Ic}^2 values.

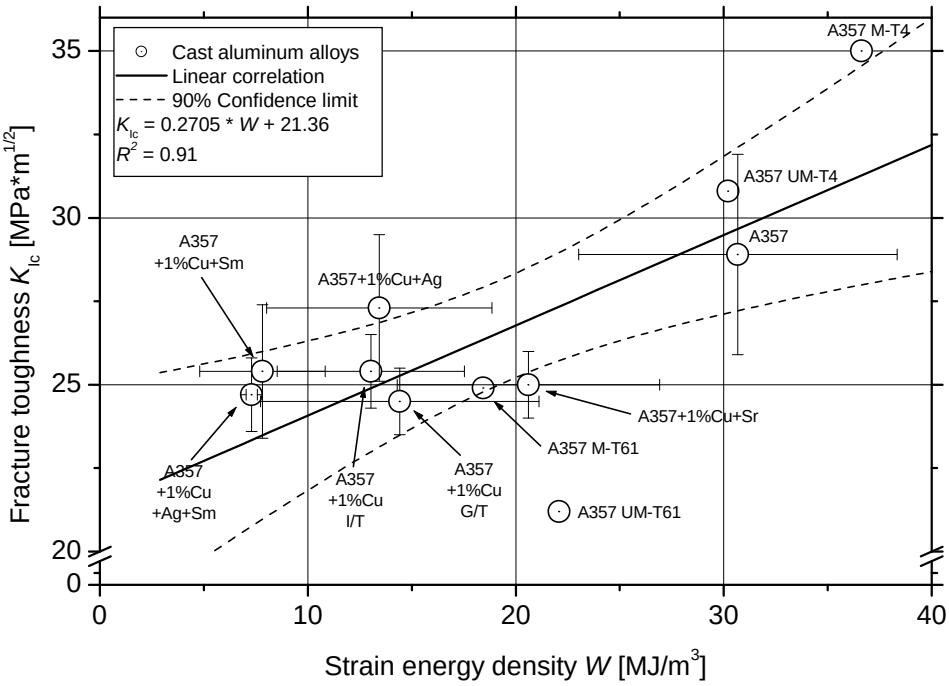

Figure 17: Correlation between strain energy density W and fracture toughness K_{Ic} values.

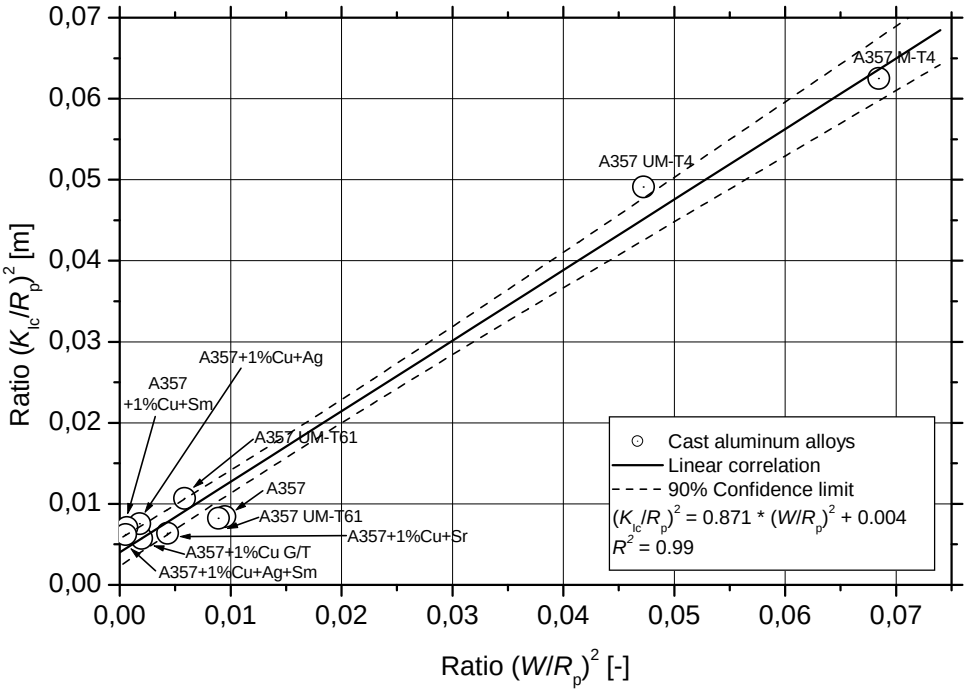

Figure 18: Correlation of the plot of the ratio $\left(\frac{K_{Ic}}{R_p}\right)^2$ over the ratio $\left(\frac{W}{R_p}\right)^2$ values.

List of Tables

54

Table 1: Heat treatment conditions of the investigated A357 cast aluminum alloys with minor chemical modifications.

Heat Treatment Code	Cast aluminum alloys	Solid solution conditions	Artificial aging
A	A357	22 h at 538°C	20 h at 155°C
B	A357+1% Cu	6 h at 500°C + 4 h at 530°C + 40 h at 535°C	8 h at 170°C
	A357+1% Cu+Sm		
	A357+1% Cu+Sr		
C	A357+1% Cu+Ag	4 h at 495°C + 4 h at 520°C + 40 h at 525°C	8 h at 170°C
	A357+1% Cu+Ag+Sm		

Table 2: Dendrite arm spacing (DAS) measurements of as-cast plates with varying thickness.

	Dendrite Arm Spacing - DAS [μm]		
Material thickness	A357 SOPHIA process	A357 normal process	A357+1% Cu SOPHIA process
5 mm	45.3	68.5	40.2
10 mm	46.9	75.1	50.4
20 mm	47.4	77.2	54.3
30 mm	50.0	-	55.7

Table 3: Mechanical properties of the investigated A357 cast aluminum alloys with (a) different artificial aging heat treatment conditions and (b) minor chemical modifications.

Cast aluminum alloys	R_p [MPa]	R_m [MPa]	A_g [%]	A_f [%]	A [%]	W [MJ/m^3]	E [GPa]	n [-]	H [MPa]
Solid solution	132	254	17.90	18.40	18.92	41.55	71.667	0.2066	148.63
06 hrs @ 155°C	160	277	17.80	19.52	19.78	49.38	72.733	0.1745	178.02
12 hrs @ 155°C	225	313	14.16	15.43	15.79	44.85	72.200	0.1189	239.50
16 hrs @ 155°C	227	315	14.13	15.39	15.73	45.36	74.300	0.1167	240.46
20 hrs @ 155°C	232	317	12.93	13.58	14.02	40.31	73.929	0.1133	245.26
24 hrs @ 155°C	255	327	11.80	12.69	13.06	38.49	73.017	0.0920	268.96
30 hrs @ 155°C	265	333	11.25	11.79	12.21	37.43	72.533	0.0837	278.06
36 hrs @ 155°C	281	338	10.21	10.60	10.97	34.66	72.533	0.0680	293.35
48 hrs @ 155°C	311	344	6.85	7.47	7.86	25.71	74.200	0.0460	323.82
Solid solution	132	254	17.90	18.40	18.92	41.55	71.667	0.2066	148.63
01 hr @ 175°C	154	276	19.90	21.12	21.64	53.60	71.855	0.1855	170.61
03 hrs @ 175°C	190	292	16.84	17.68	18.18	48.36	72.165	0.1462	203.76
06 hrs @ 175°C	259	323	11.74	12.75	13.28	40.28	70.242	0.0784	273.38
09 hrs @ 175°C	287	338	9.57	10.52	11.05	35.45	71.560	0.0549	303.18
12 hrs @ 175°C	296	340	8.57	9.73	10.29	33.07	73.874	0.0494	308.71
20 hrs @ 175°C	304	344	6.87	7.42	7.95	25.81	72.055	0.0465	320.12
36 hrs @ 175°C	295	333	6.47	7.53	8.00	25.45	72.628	0.0438	309.56
48 hrs @ 175°C	311	344	6.08	6.37	6.91	22.45	72.234	0.0357	325.35
Solid solution	132	254	17.90	18.40	18.92	41.55	71.667	0.2066	148.63
01 hr @ 205°C	267	325	10.09	11.27	11.83	36.10	70.197	0.0717	280.73
02 hrs @ 205°C	293	338	7.92	8.63	9.16	29.17	72.259	0.0491	308.01
03 hrs @ 205°C	301	336	7.07	8.33	8.88	28.39	70.918	0.0416	314.25
04 hrs @ 205°C	286	325	7.41	9.24	9.79	30.27	71.697	0.0395	299.32
05 hrs @ 205°C	281	327	7.78	9.19	9.66	29.96	72.432	0.0390	295.80
06 hrs @ 205°C	291	321	6.26	8.13	8.65	26.68	71.780	0.0374	302.46
10 hrs @ 205°C	292	325	6.79	8.41	8.92	27.80	72.719	0.0342	305.12
12 hrs @ 205°C	304	334	6.23	8.60	9.19	29.43	71.830	0.0322	317.26
16 hrs @ 205°C	300	332	6.47	9.24	9.74	30.99	72.714	0.0308	315.05
24 hrs @ 205°C	257	285	4.02	5.05	5.50	14.58	69.351	0.0571	266.33
36 hrs @ 205°C	216	250	4.76	7.48	7.86	18.42	68.302	0.0775	226.74

(a)

Cast aluminum alloys	R_p [MPa]	R_m [MPa]	A_f [%]	W [MJ/m^3]	E [GPa]	n [-]	H [MPa]	K_{Ic} [MPa$\sqrt{m}$]
A357	315	368	8.14	30.68	74.750	0.0781	485.71	28.9
A357+1% Cu I-T	317	369	3.34	13.03	76.882	0.0328	426.30	25.4
A357+1% Cu G-T	323	379	3.58	14.42	76.222	0.0350	441.68	24.5
A357+1% Cu+0.7% Ag	314	373	3.41	13.44	75.476	0.0335	431.80	27.3
A357+1% Cu+0.5% Sm	302	341	2.11	7.82	76.059	0.0208	376.82	25.4
A357+1% Cu+Ag+Sm	314	368	1.80	7.30	72.667	0.0178	402.51	24.7
A357+1% Cu+Sr	313	368	5.40	20.61	69.558	0.0525	451.84	25.0
Á357 UM-T4 [4]	139	266	11.95	*30.21	72.278	*0.1129	*380.93	30.8
A357 M-T4 [4]	140	265	14.69	*36.63	70.794	*0.1371	*399.08	35.0
A357 UM-T61 [4]	234	311	7.34	*22.08	74.637	*0.0708	*402.68	21.2
A357 M-T61 [4]	241	312	6.08	*18.44	71.532	*0.0590	*391.13	24.9

* calculated properties by exploiting approximate equations presented in [32]

(b)